Experimental study of the mold flow induced by a swirling flow nozzle and electromagnetic stirring for continuous casting of round blooms

Schurmann, D.; Willers, B.; Hackl, G.; Tang, Y.; Eckert, S.;

Originally published:

March 2019

Metallurgical and Materials Transactions B 50(2019)2, 716-731

DOI: https://doi.org/10.1007/s11663-018-1491-5

Metallurgical and Materials Transactions B manuscript No.
(will be inserted by the editor)

Experimental study of the mold flow induced by a swirling flow nozzle and electromagnetic stirring for continuous casting of round blooms

Dennis Schurmann · Bernd Willers · Gernot Hackl · Yong Tang · Sven Eckert

Received: 20.09.2018 / Accepted: 17.12.2018

Abstract This study focuses on an experimental investigation of the fluid flow in round bloom continuous casting using a 1:3 model of the industrial casting process. A swirling flow nozzle, represented by the specific design of the RHI Magnesita GYRONOZZLE, is used to produce a swirling motion in the cylindrical mold. The test section is integrated in the Mini-LIMMCAST facility at HZDR, which is operated at room temperature using the ternary alloy GaInSn. Systematic measurements of horizontal and vertical velocity profiles are performed by means of the Ultrasound Doppler Velocimetry (UDV). The second part of the study focuses on the interaction between the flow driven by the GYRONOZZLE and concurrent electromagnetic stirring in the mold (M-EMS) by applying rotating magnetic fields (RMF) at different magnetic flux densities. The effect of the GYRONOZZLE on the flow pattern inside the mold is examined with and without superimposed RMF and compared to those of a standard single-port nozzle. The measurements reveal that the GYRONOZZLE induces a swirling flow in the whole mold. It is further shown that the influence of a simultaneously applied RMF is mainly restricted to the lower part of the mold since the transport of angular momentum to the top is suppressed by the jets pouring out from the GYRONOZZLE.

Keywords Continuous Casting · Round Bloom Casting · Swirling Flow Nozzle · Liquid Metal Model Experiments · Flow Measurements · Ultrasound Doppler Velocimetry (UDV)

Dennis Schurmann · Bernd Willers · Sven Eckert
Helmholtz-Zentrum Dresden-Rossendorf e.V. (HZDR),
Bautzner Landstraße 400, 01328 Dresden, Germany
E-mail: d.schurmann@hzdr.de

Gernot Hackl · Yong Tang
RHI Magnesita, 8700 Leoben, Austria

1 Introduction

Over the past few years, research activities and technological development on optimizing continuous casting with respect to high process efficiency and excellent product quality have focused increasingly on controlling the fluid flow in the tundish, the submerged entry nozzle (SEN) and the mold. It is well-known that serious casting defects could arise from adverse flow patterns and the unpredictable nature of highly turbulent flows. Violent behavior of the submerged jets, transient vortex structures, low-frequency oscillations of the global flow pattern or turbulent flow near the meniscus endanger the quality of the cast product. In particular, single-port SENs, as they are commonly used in billet casting, produce a strong downward flow in the mold that makes the flotation and removal of inclusions and bubbles difficult. In general, two different strategies are applied for flow control in continuous casting: on the one hand, the process design is improved in terms of an optimal geometry and arrangement of components such as the tundish or the SEN, and on the other hand, diverse electromagnetic actuators are used to achieve contactless tailoring of the fluid flow.

Especially for the production of round and square cast geometries, a swirling flow in the SEN and the mold is considered beneficial for product quality. This approach is motivated by the following expectations: (I) a reduction of the penetration depth of the jet exiting the SEN, (II) a stabilization and homogenization of the flow pattern in the mold, (III) promoting the heat and mass transfer in regions beneath the meniscus, (IV) reducing the surface defects of the steel product, and (V) a prevention of nozzle clogging [36, 37]. Furthermore, an intense stirring and the generation of shear flows in the solidification region is supposed to promote grain refinement and the transition from columnar to equiaxed solidification [23, 32]. A swirling flow can be produced by electromagnetic stirring (EMS) applied either at the mold

(M-EMS) [9, 22, 30] or at the SEN [13, 33–35, 38]. Regardless of the fact that electromagnetic stirring is an extremely flexible and smart contactless method, the installation and operation of an electromagnetic stirrer causes additional investment and energy costs to the operator. Therefore, alternative variants are considered to reduce these costs and to minimize the energy consumption. Rotating flows in the nozzle can also be generated by installing inserts in the SEN [36, 37] or the tundish [16–19].

Various nozzle designs have already been tested in terms of their efficiency in creating a rotating flow in the mold. For instance, the insertion of swirl blades in the SEN was proposed by Yokoya et al.[36, 37]. The authors claim a couple of positive effects such as a reduction of the penetration depth of the nozzle outlet flow, a uniform velocity distribution in a short distance from the nozzle port or an activation of the heat and mass transfer near the meniscus. Another variant is the combination of swirl blades and a gradual divergence of the nozzle cross section [37, 38]. Although the tangential velocities achieved in this configuration are relatively low in the nozzle, the authors nonetheless observed a noticeable reduction of the maximum velocities both near the nozzle outlet and the free surface. Moreover it was reported that the concept of swirl blades in the SEN combined with a suitable design of the outlet ports was tested successfully with measurable results under industrial conditions [29].

A different approach is to generate a swirling flow in the tundish using a special cylindrical design [16–19]. Here, the idea is to achieve a similar effect as in case of the swirl blades by simply modifying the flow structure in the tundish. Therefore, the authors claim a very efficient method of swirl generation because additional installations for flow conditioning are not needed.

Sun et al. [24] applied a four port nozzle with horizontal outlets where its azimuthal orientation is chosen in such a way that the jets impinge obliquely on the inner wall. The redirection of the jets at the wall is supposed to be responsible for the development of a swirling flow in the mold. The outcome of this study is essentially based on numerical simulations. Accompanying plant trials were reported where the swirling flow caused an improvement of the product quality in terms of a reduction of porosity compared to a single-port nozzle. In case of a concurrent application of the swirling nozzle and a M-EMS the authors recommend opposite rotating directions for eliminating segregation zones.

A contactless generation of a rotating flow in the submerged entry nozzle by means of an electromagnetic stirrer which is positioned around the SEN is investigated by several researchers [13, 33–35, 38]. Positive effects were also demonstrated for this arrangement, but at first glance the effort with regard to an electromagnetic stirrer appears to be higher than in comparison to simple structural changes in the nozzle. Apart from that, a nozzle without mechanical inserts has a lower probability for clogging [29].

The submerged entry nozzle design under investigation in this study, the RHI Magnesita GYRONOZZLE [6, 7], is developed to improve the flow conditions in billet and bloom molds. The helical port design of this nozzle type imposes a rotating flow pattern in the strand. It is to be expected that the GYRONOZZLE, due to its internal construction, better converts the kinetic energy of the incoming jet into a rotating flow than the four port nozzle proposed by Sun et al. [24], since in the case of the latter much energy is dissipated by the impact of the jets against the sidewall. The GYRONOZZLE is designed to avoid a deep jet penetration resulting in a higher probability for removing nonmetallic inclusions. The primary goal is to produce an efficient mixing in the upper mold region, which is supposed to result in an improvement of the strand lubrication by enhanced mold powder melting rates and in a more effective superheat dissipation. Moreover, a reduced jet impingement on the solidifying shell should be achieved in comparison to the use of conventional multi-port designs. Finally, the question arises, to what extent can the GYRONOZZLE replace the use of an M-EMS, or can an optimal process control be achieved by means of a suitable combination of GYRONOZZLE and electromagnetic stirring.

Most previous experimental studies were restricted to flow measurements in water models. The Mini-LIMMCAST model facility enables detailed investigations in liquid metal flows. The liquid metal model experiments allow for a quantitative comparison between swirling nozzle and mold electromagnetic stirrer (M-EMS) under the same experimental conditions. Moreover, this study presents the first flow measurements for a combined application of swirling nozzle and electromagnetic stirring.

2 Experimental setup

2.1 Experimental facility

The experiments presented here were performed at the Mini-LIMMCAST facility at HZDR [26–28]. This facility is used for investigations of flow phenomena and associated transport processes in the continuous casting process of steel. It is operated at room temperature with the ternary eutectic alloy GaInSn whose thermo-physical properties [20] are close to those of steel (cf. Tab. 1). The present study concerns the isothermal flow in a 1:3 scale PMMA model of a round bloom industrial caster equipped with an electromagnetic stirrer [31]. Figure 1 shows a schematic drawing of the Mini-LIMMCAST facility and relevant components of the test section such as tundish, submerged entry nozzle and mold, while Table 2 lists the most important model dimensions as well as the parameters of the electromagnetic stirrer (EMS).

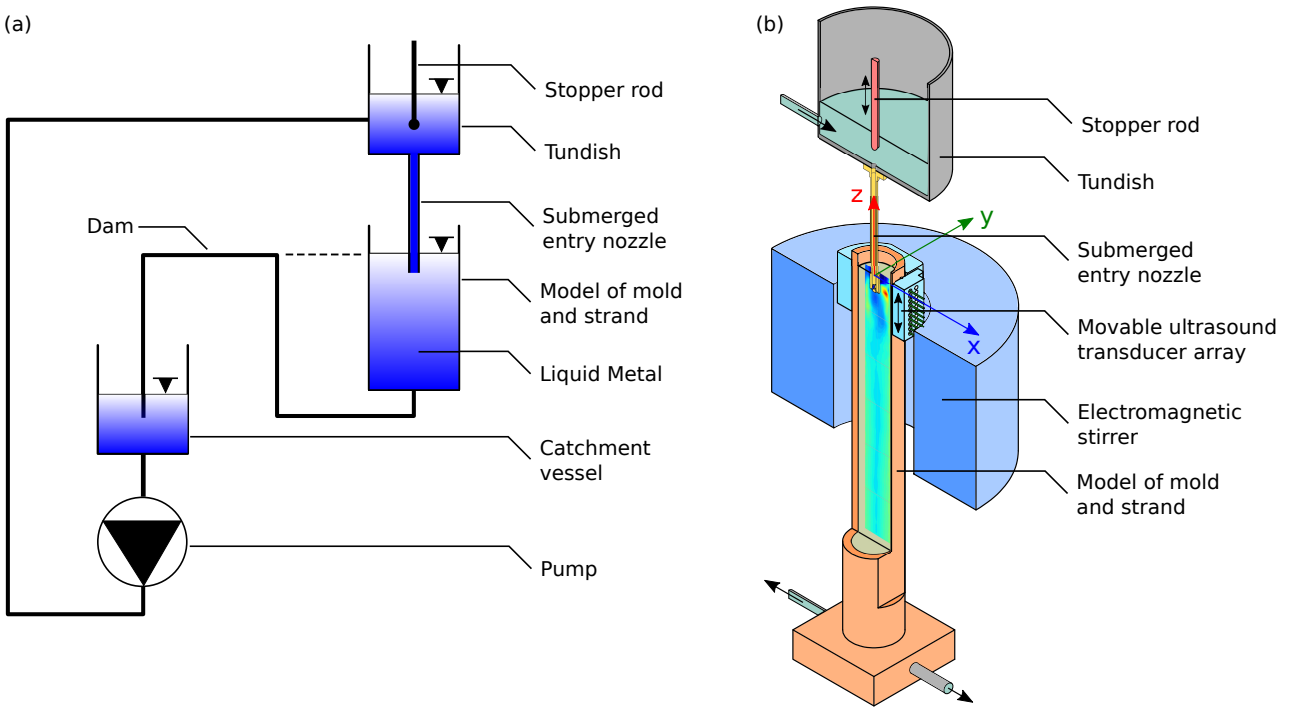

Fig. 1 Schematic representation of (a) the liquid metal loop, and (b) the round test section, representing the round mold and strand, the submerged entry nozzle (GYRONOZZLE), the electromagnetic stirrer and the movable ultrasound transducer array. A contourplot shows a sample result obtained in this configuration.

The test section is integrated into a loop system with storage tank and electromagnetic pump. The liquid metal flow rate from the tundish into the mold is regulated by a stopper rod at the entrance of the SEN. From the mold, the liquid drains over a dam, whose position simultaneously determines the height of the free surface in the mold, into a storage vessel. From the storage tank, the fluid is continuously pumped back into the tundish, whereby long-term measurements become possible.

The cylindrical mold is made of PMMA with an inner diameter of 80 mm and a length of approx. 800 mm. One side of the mold wall has been milled even to allow measurements through the wall. The position of the free surface of the liquid metal in the mold is kept constant and is defined as $z = 0$. Both, a xyz- and a $r\varphi z$-coordinate system are used to represent the geometry of the mold and the positioning and alignment of the ultrasound transducers and the velocity components to be measured. For reasons of brevity coordinates are abbreviated, e.g. $y = 15\,\text{mm} \rightarrow y15$.

The model of the submerged entry nozzle has been 3D printed and supplied by RHI Magnesita (see Fig. 2). It is a swirling flow nozzle and available under the product name GYRONOZZLE. The inner diameter of the nozzle is 10 mm, while the outer diameter is 20 mm. The nozzle has four ports, each twisted by an angle of 34° in mathematically positive direction from top to bottom, resulting in a swirl flow in

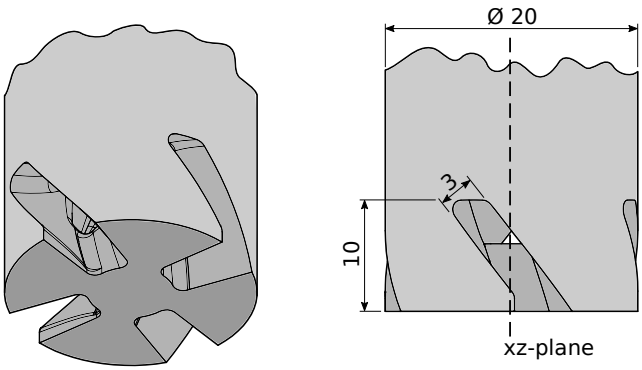

Fig. 2 3D CAD representation of the geometry of the submerged entry nozzle (RHI Magnesita GYRONOZZLE) and its alignment to the coordinate-system of the setup.

the mold, which is also directed in mathematically positive direction. The lower edge of the SEN is positioned at $z = -35\,\text{mm}$. The GYRONOZZLE is mounted vertically and aligned in azimuthal direction so that the center of the ports match with the xz- and yz-planes of the coordinate system.

An electromagnetic stirrer is placed around the mold (M-EMS) to produce a rotating magnetic field (RMF) at a frequency of 2.5 Hz and magnetic flux densities up to $B_0 = 18.3\,\text{mT}$. More details of the magnetic system can be found

Table 1 Physical properties of liquid steel [8, 10, 11, 14] and GaInSn [20].

Property	Symbol	Unit	Liquid Steel	GaInSn
reference temperature	T	°C	~ 1500	20
density	ρ	$\mathrm{kg/m^3}$	$\sim 7\,000$	6 353
dynamic viscosity	η	$\mathrm{kg/(ms)}$	~ 0.002 ... 0.018	0.00218
electrical conductivity	σ	$1/(\Omega\mathrm{m})$	$\sim 0.833 \times 10^6$	3.29×10^6
thermal conductivity	λ	$\mathrm{W/(mK)}$	~ 30	23.98
surface tension	γ	$\mathrm{N/m}$	~ 1.7	0.587

Table 2 Overview of model dimensions.

Property	Value
Model of Mold and Strand	
inner diameter	80 mm
height	800 mm
Submerged Entry Nozzle (SEN)	
inner diameter	10 mm
outer diameter	20 mm
position of lower edge	−35 mm
number of ports	4
port height	10 mm
port width	3 mm
port twist angle	34°
Electromagnetic Stirrer (EMS)	
inner diameter	200 mm
outer diameter	495 mm
height	310 mm
position of center	−225 mm
frequency	2.5 Hz
max. magn. flux density	18.3 mT

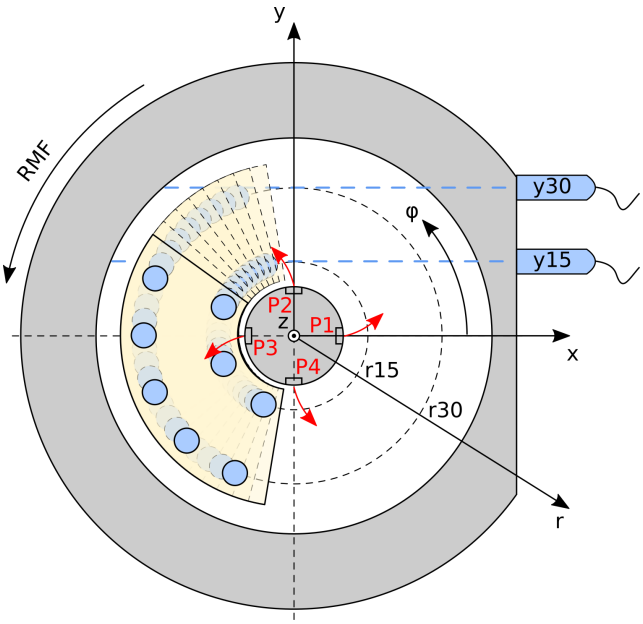

Fig. 3 Schematic representation of the positioning of the horizontally and vertically aligned ultrasound transducers used in this study. The positions of the vertical velocity measurement segment are shown. The four ports of the GYRONOZZLE are indicated by P1 to P4.

in [31]. The stirrer's top edge is positioned at $z = -70\,\mathrm{mm}$, the center of the stirrer is located at $z = -225\,\mathrm{mm}$.

2.2 Measurement setup

The Ultrasound Doppler Velocimetry (UDV) was applied in this study to measure the flow structure in the opaque liquid metal flow. For a description of the measuring principle we refer to [2]. Velocity profiles were recorded at various locations inside the mold by the DOP 3010 instrument (Signal Processing SA, Switzerland [21]). The device was equipped with up to ten ultrasonic (US) transducers with a piezo diameter of 5 mm and a emitting frequency of 4 MHz. Each transducer measures the projection of the fluid velocity on the propagation direction of the ultrasonic beam. The parallel alignment and repeated sequential polling of several transducers enables a two dimensional spatio-temporal flow mapping of the velocity component in beam direction. Therefore $v_{b,i}(b,t)$, the spatio-temporal representation of the velocity for US-sensor i recorded at a distance b in beam direction and time step t, is recorded.

The velocity value at each distance b from the transducer is determined for a cylindrical measuring volume whose size depends on the propagation properties of the ultrasound in the respective material. Due to the divergence of the ultrasonic beam the radial dimension of the measuring volume increases with increasing distance from the transducer. Taking into account the calculated half opening angle of $\gamma_{-3\,\mathrm{dB}} = 2.9°$ in GaInSn [12], the radial dimension of the measuring volume in a distance of 100 mm from the transducer would be approx. 7.6 mm. The spatial resolution in axial direction is less than 1 mm.

The ultrasonic sensors were placed on the outside of the PMMA mold wall or in direct contact with the liquid metal. Since PMMA has a comparable speed of sound as

Table 3 Experimental matrix showing the combination of the parameters v_{SEN} and B_0 on which the analysis focused in this study. The sign + represents the application of the respective magnetic flux density B_0 in the same direction as the SEN-port direction, while ±-sign represents measurements where stirring in both directions was applied. v_{cast} is the mean velocity in the strand, obtained by multiplying v_{SEN} with the cross-section ratio between SEN and mold.

v_{SEN}	v_{cast}	B_0 [mT]						
m/s	m/min	0	7.5	10.6	13.0	15.0	16.7	18.3
1.2	1.1	+	+	+	+	+	+	+
1.4	1.3	+						
1.8	1.7	+						
2.1	2.0	+	±					±

GaInSn ([3, 15]), no disturbances of the measurements due to diffraction effects are to be expected.

In this study the velocity vector **v** in mold and strand is described by the three velocity components u, v and w pointing in the direction of the Cartesian coordinate axes ($\mathbf{e_x}$, $\mathbf{e_y}$ and $\mathbf{e_z}$ respectively):

$$\mathbf{v} = u\mathbf{e_x} + v\mathbf{e_y} + w\mathbf{e_z} \tag{1}$$

2.3 Measurement procedure

Our investigations are based essentially on systematic measurements of the horizontal and vertical velocity components in the mold, u and w respectively. The different locations of the transducers can be seen in Fig. 3. The mean velocity of the flow in the SEN v_{SEN} was measured by positioning a sensor at an angle of 30° at the outside of the SEN. The mean flow velocity in the SEN was varied by opening the stopper rod to a certain height. The control system of the Mini-LIMMCAST facility guaranteed that the liquid metal level in the tundish was always kept at a constant value of 50 mm above the tundish bottom. Flow speeds between 0.6 m/s and 2.1 m/s were achieved.

2.3.1 Horizontal velocities

Horizontal velocity profiles u have been acquired by placing two times ten ultrasound-sensors with a vertical spacing of $\Delta z = 10$ mm in a movable array at the outside of the PMMA mold wall at positions of $y = 15$ mm and 30 mm ($y15$ and $y30$ respectively, cf. 3). The measurements at $y15$ and $y30$ were conducted in succession. The entire height of the mold was covered by sequentially shifting the sensor array to six different vertical positions. The highest sensor position was at $z = -5$ mm, while the lowest position was at $z = -595$ mm.

The horizontal velocities presented within this paper were obtained for various values of $v_{SEN} \leq 2.1$ m/s (see Table 3). The RMF was applied with different magnetic flux densities B_0 for the lowest and highest flow rate. The measurements at $v_{SEN} \approx 1.2$ m/s were performed with a RMF rotating in the same direction as the nozzle swirl while at $v_{SEN} \approx 2.1$ m/s the RMF was applied in the same direction as the nozzle swirl as well as in opposite direction (counter-stirring). After setting a new magnetic field strength, a minimum interval of 2 minutes has been waited before continuing the measurements in order to allow the system to adapt to the new parameters.

Additionally, high resolution measurements, which enable more features of the flow structures to be identified, have been performed directly under the free surface using an advanced UDV-array measurement system which contains 25 piezoelectric transducers in a compact body [4, 5].

2.3.2 Vertical velocities

Measurements of the vertical velocity profiles w were performed in a configuration where eight transducers were placed in a circular segment (see Fig. 3). The measurements were conducted for the highest flow speed in the SEN of $v_{SEN} \approx 2.1$ m/s with and without a counter-stirring RMF of 18.3 mT.

The transducers were placed in the vicinity of port P3 immersed into the liquid metal to a depth of 10 mm at radial positions of $r = 15$ mm and 30 mm ($r15$ and $r30$ respectively). The angular spacing between the sensors was $\Delta\varphi_{r15} = 22.5°$ and $\Delta\varphi_{r30} = 11.125°$. After each measurement, the circular segment was moved by $\Delta\varphi = 5.6°$. By moving the segment eight times a total measurement range of 135° from $\varphi = 112.5°$ to 247.5° has been recorded. Data from sensor positions that were measured multiple times, due to $\Delta\varphi_{r30} < \Delta\varphi_{r15}$, were averaged.

3 Results

3.1 Visualization of the jets

Fig. 4 shows a photograph of the liquid metal jets emerging from the ports of the GYRONOZZLE. The liquid metal level in the mold is lowered so that the SEN is not submerged and the jets become visible. The photograph provides an impression of the shape of the jets, while the jets' shape is likely to be different in the real operating regime due to the interaction with the liquid metal in the mold.

It can be observed that the jets exit the SEN at an angle of approx. 45°. After contact with the mold wall the metal flows mainly downward, but also partly upwards. It can be further seen that the swirl of the jets is generated by the lower edge of the GYRONOZZLE ports, while a second part of the jet exits the port more vertically. Moreover, the nozzle ports are not filled completely by the liquid metal jets.

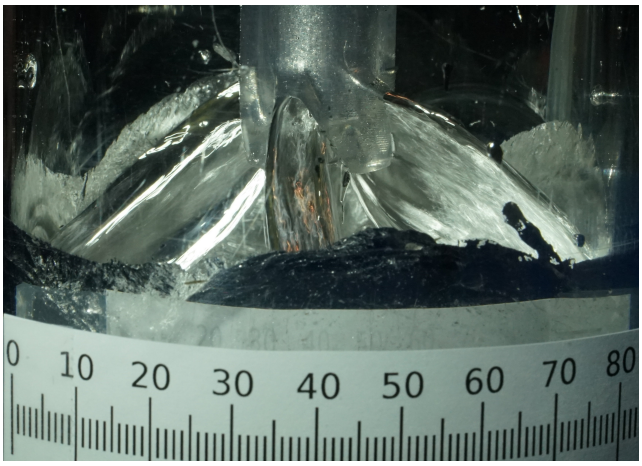

Fig. 4 Photograph of the liquid metal jets emerging from the ports of the GYRONOZZLE. For this demonstration, the liquid metal level in the mold was lowered below the nozzle position. The scale is placed on the outside of the PMMA mold.

3.2 Measurements of the horizontal velocities

3.2.1 Horizontal mold flow without RMF

Fig. 5 shows three contourplots of the time-averaged measured horizontal velocity distribution u in the mold at $y = 15\,\mathrm{mm}$ for three different velocities in the SEN. The two-dimensional flow fields were obtained by interpolation based on the data measured at the vertical sensor positions along the mold height. The ultrasound was emitted from the right side of the mold (see Fig. 3).

In general, the contour plots reveal the existence of three zones in the mold characterized by different flow patterns. The upper part of the mold above the nozzle ports ($z \geq -30\,\mathrm{mm}$) is completely occupied by a continuous swirling motion where the highest negative velocities occur just under the free surface in the central part between $x = \pm 20\,\mathrm{mm}$. In contrast, the flow field in the region below the nozzle ($-30\,\mathrm{mm} > z > -125\,\mathrm{mm}$) is more complicated. Negative velocities, that would fit a mathematical positive rotation, can only be observed in the inner core around the axis, whereas opposite flow directions can be observed in the peripheral areas. Finally, a dominating swirling motion of lower intensity with a sense of rotation that corresponds to the direction of the exiting jets can be found in the lower part of the mold ($z < -125\,\mathrm{mm}$). It becomes obvious that the mean intensity of the flow throughout the mold increases with increasing flow rate.

Fig. 6 contains a flow distribution close to the free surface and the nozzle ports, measured by the ultrasonic array with a higher spatial resolution in z-direction. A distinct area of high positive velocities u can be found at $x \approx 22\,\mathrm{mm}$, $z \approx -45\,\mathrm{mm}$, which is caused by the jet from port P1 moving towards the wall in this region. The measuring plane cuts the jet from port P2 at $x \approx -4\,\mathrm{mm}$, $z \approx -35\,\mathrm{mm}$. Since the jet has just left the SEN here, it appears in the contour plot as a narrow zone of negative velocity. The twisted form of the jets explains the occurrence of high values of the horizontal velocity at the position $x \approx -4\,\mathrm{mm}$ and why this jet appears at a higher position than the jet from port P1. The latter crosses the measurement plane in a greater horizontal and vertical distance from its port position. In direct vicinity to the jet from port P2, at $z = -35\,\mathrm{mm}$, a strong gradient of u becomes obvious. The sign change of the velocity indicates the formation of a recirculation zone and strong shear stress close to the jets. A similar counter flow can be observed close to the jet from port P1 at $x \approx 32\,\mathrm{mm}$, $z \approx -35\,\mathrm{mm}$. A zone of negative velocities exists below the nozzle $-25\,\mathrm{mm} \leq x \leq 20\,\mathrm{mm}$ indicating the rotating core driven by the jets. The high negative velocity at $x = -10\,\mathrm{mm}, z = -45\,\mathrm{mm}$ might result from the part of the jet from port P2 which exits the port more vertically. The two areas of low velocities in the upper part at $x = 5\,\mathrm{mm}$ and $-25\,\mathrm{mm}$, $z > -30\,\mathrm{mm}$ are artifacts resulting from a steady echo signal reflected by the SEN. These artifacts are not present in the measurements with single transducers probably due to their different ultrasonic beam characteristic and the distinct signal processing of their echo signal.

For a quantitative comparison of the velocities in the mold under different operating conditions, the horizontal velocity component $u_{x0} = u(x = 0)$ has been extracted from the measurement data. The velocity component $u_{x0,y15}$ corresponds to the circumferential velocity component $v_\varphi(\varphi = 90^\circ, r = 15\,\mathrm{mm})$.

The relation between the velocity in the submerged entry nozzle v_{SEN} and the resulting time-averaged velocities ($u_{x0,y15}$ and $u_{x0,y30}$) for the ten highest z-positions in the mold is displayed in Fig. 7. By adjusting the position of the stopper rod, the mean velocity v_{SEN} was varied in the range from $0.6\,\mathrm{m/s}$ to $2.1\,\mathrm{m/s}$.

It is obvious that the azimuthal velocities in the upper part of the mold increase linearly with increasing v_{SEN}. The highest velocities can be found at $y15$ directly underneath the free surface at $z = -5\,\mathrm{mm}$, whereas the lowest velocities are observed at $z = -45\,\mathrm{mm}$, which is directly below the SEN. The rotation of the fluid at $y15$ (Fig. 7a) is significantly higher at the four positions from the free surface to the lower edge of the SEN than it is deeper in the mold. The tendency of decreasing azimuthal velocities with increasing depth in the mold can also be observed at $y30$ (Fig. 7b), but the differences are smaller here, and there is no sudden change between the regions above and below the lower edge of the SEN.

It is worth noting that in the region beneath the surface higher velocities are detected at $y15$, i.e. at the measurement position close to the center of the mold, as in the outer zones near the side walls at $y30$. This shows that in this area no solid-body rotation occurs, in which the velocity would have

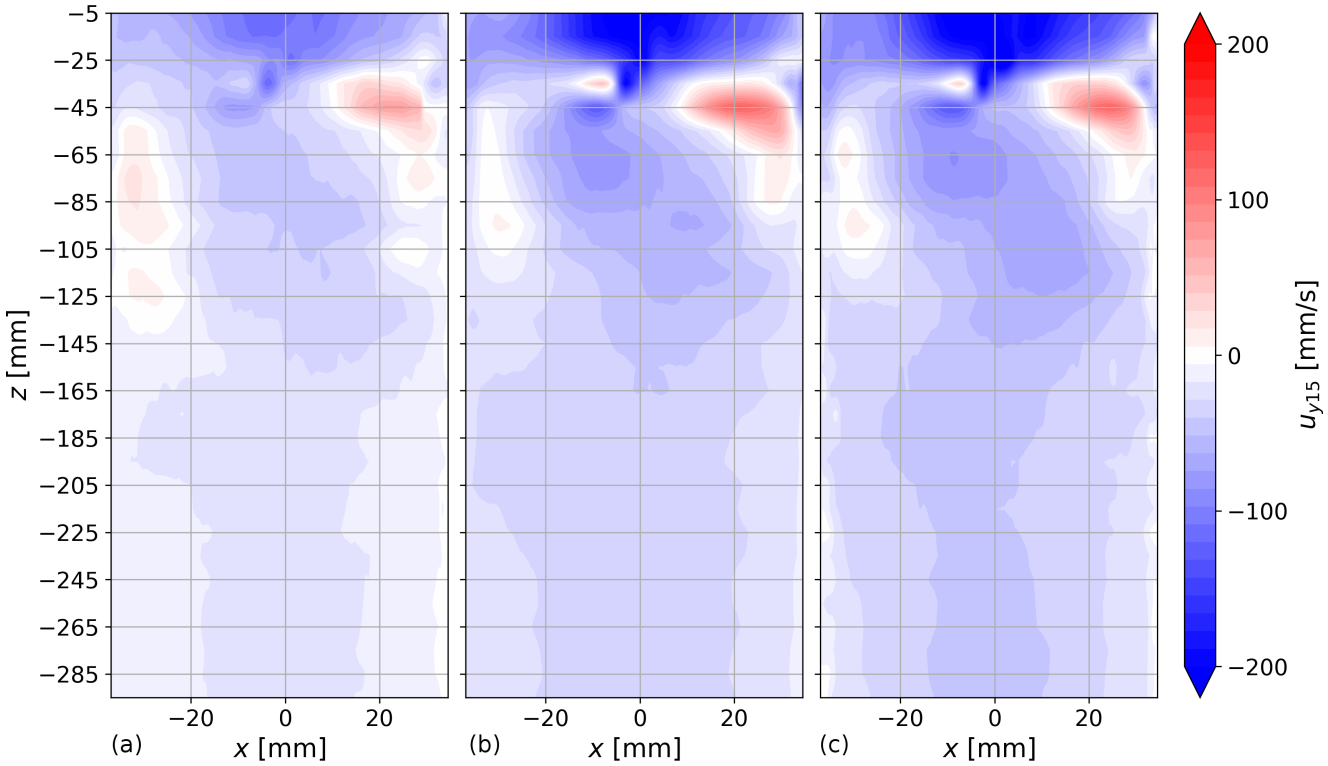

Fig. 5 Contour plots of the time-averaged velocity distribution along the mold height at $y = 15\,\text{mm}$ without RMF for different velocities in the SEN a) $1.2\,\text{m/s}$, b) $1.8\,\text{m/s}$ and c) $2.1\,\text{m/s}$.

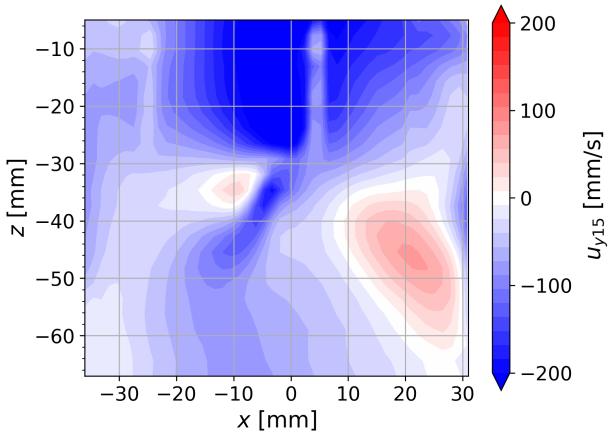

Fig. 6 High resolution measurement of the time-averaged horizontal velocity u close to the free surface and the nozzle ports at $y = 15\,\text{mm}$ without RMF and a velocity of $1.8\,\text{m/s}$ in the SEN.

to increase linearly with the radial position. This behavior is very likely to be explained by angular momentum transport provided by the secondary flow (see also [31]).

The time-averaged velocities $u_{x0,y15}$ and $u_{x0,y30}$ along the mold height are shown in Fig. 8 for four different velocities in the SEN. As already seen in Fig. 7, the highest velocities appear underneath the free surface and increase with increasing v_{SEN}. This proportionality between azimuthal velocity and flow in the SEN also exists in the lower part of the mold.

In the center of the mold at $y15$ (Fig. 8 a)) the highest absolute velocities are detected for $v_{\text{SEN}} \approx 2.1\,\text{m/s}$ at $z = -25\,\text{mm}$ with $u_{x0,y15} = -225\,\text{mm/s}$, which is more than 5 times as much as in the lower part of the mold where values of $u_{x0,y15} = -40\,\text{mm/s}$ are found. The velocity decreases until $z = -200\,\text{mm}$ and remains relatively constant from there to the end of the measuring region at $z = -595\,\text{mm}$.

In comparison to the vertical profiles of the horizontal velocity measured at $y15$, the velocities at the outer position $y30$ (Fig. 8 b)) are slowly declining from about $-60\,\text{mm/s}$ at $z = -200\,\text{mm}$ to $-35\,\text{mm/s}$ at $z = -595\,\text{mm}$ for $v_{\text{SEN}} \approx 2.1\,\text{m/s}$. The lowest measured velocity is $u_{x0,y30} = -18\,\text{mm/s}$ at $z = -595\,\text{mm}$ with $v_{\text{SEN}} \approx 1.2\,\text{m/s}$. In both diagrams distinct local changes of the velocity are found in the upper part of the mold above $z \geq -105\,\text{mm}$. The flow in this area has a rather complex structure which is mainly caused by the three-dimensional character of the jets exiting the ports.

3.2.2 Horizontal mold flow under the influence of a co-rotating RMF

Fig. 9 shows the time-averaged horizontal velocities $u_{x0,y15}$ and $u_{x0,y30}$ with and without a co-rotating RMF of different

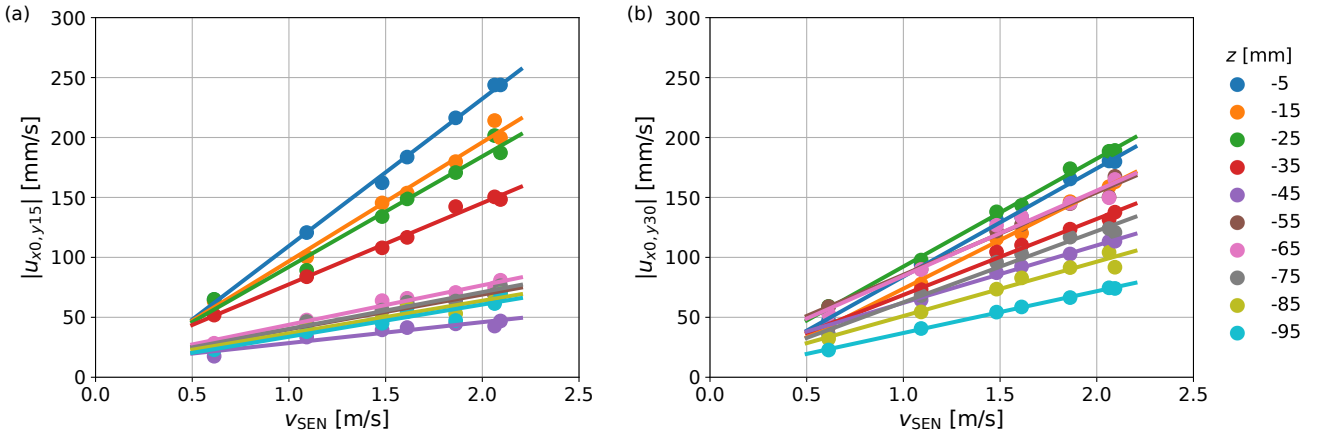

Fig. 7 Time-averaged velocities $u_{x0,y15}$ and $u_{x0,y30}$ at the first ten z-positions under the free surface with variable velocities in the SEN v_{SEN}, measured at a) $y = 15\,\text{mm}$ and b) $y = 30\,\text{mm}$.

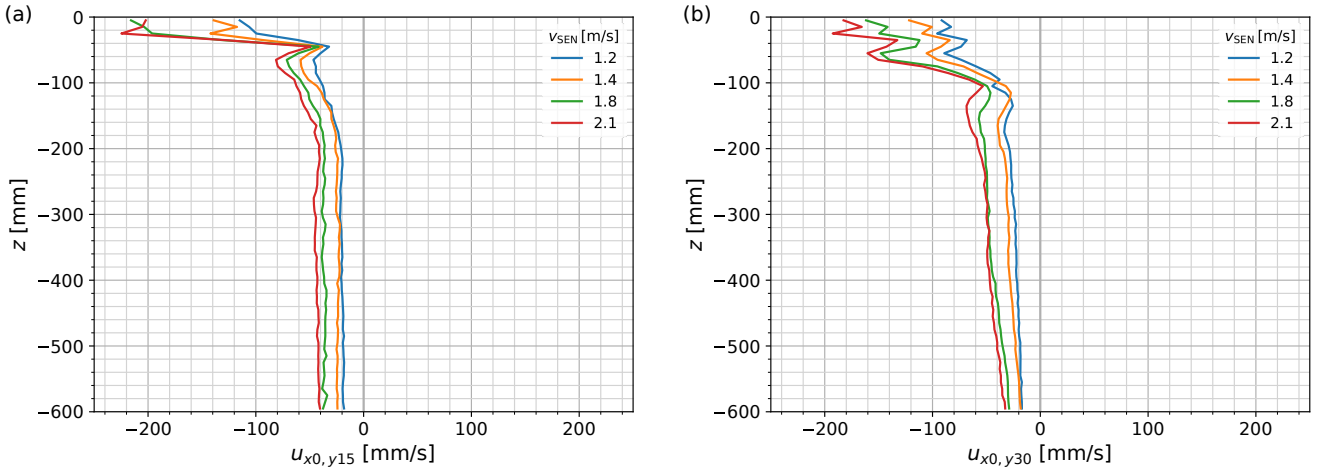

Fig. 8 Time-averaged velocities $u_{x0,y15}$ and $u_{x0,y30}$ along the mold height without RMF with varying casting speeds v_{SEN} measured at a) $y = 15\,\text{mm}$ and b) $y = 30\,\text{mm}$.

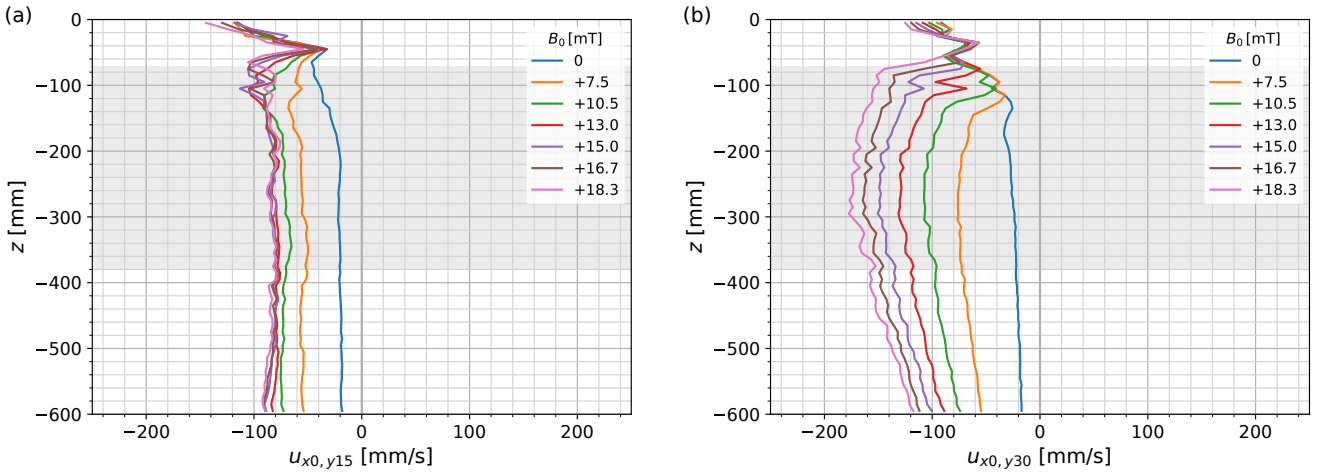

Fig. 9 $u_{x0,y15}$ and $u_{x0,y30}$ with $v_{SEN} \approx 1.2\,\text{m/s}$ and stirring in the same direction with different magnetic flux densities B_0 measured at a) $y = 15\,\text{mm}$ and b) $y = 30\,\text{mm}$.

magnetic flux densities up to $B_0 = 18.3\,\mathrm{mT}$ for a SEN velocity of $v_{\mathrm{SEN}} \approx 1.2\,\mathrm{m/s}$. The position of the stirrer ($-380\,\mathrm{mm} \leq z \leq -70\,\mathrm{mm}$) is marked by a gray background shade in the diagrams.

Considering the deeper positions in the mold below the SEN ($z \leq -60\,\mathrm{mm}$), the RMF application raises the rotation rate at the measurement position close to the center of the mold ($y15$, Fig. 9 a)), while velocity differences along the mold height are almost negligible. The velocities increase from about $-20\,\mathrm{mm/s}$ for the GYRONOZZLE case without RMF to values up to approx. $-80\,\mathrm{mm/s}$. However, a type of saturation effect can be noted, i.e. an increase of the magnetic field strength beyond a value of $B_0 \geq 13\,\mathrm{mT}$ does not lead to a further acceleration of the swirling flow in the bulk. The velocities under the free surface are only marginally increased by an applied RMF.

The horizontal velocity distributions u plotted for $y30$ in Fig. 9 b) demonstrate a significant and continuous increment of the azimuthal flow with increasing field strength at vertical positions below the SEN. In particular, the RMF affected zone expands to the top with increasing B_0. For a RMF of $B_0 \geq 10.5\,\mathrm{mT}$ the highest velocities no longer occur under the free surface, but in the lower part of the mold. The effect of the electromagnetic stirring on the velocities in close vicinity to the free surface at $y30$ appears to be rather low.

The specific arrangement of the velocity profiles in Fig. 10 taken from experiments with $v_{\mathrm{SEN}} \approx 1.2\,\mathrm{m/s}$ and $2.1\,\mathrm{m/s}$ carried out with and without an RMF of $B_0 = 18.3\,\mathrm{mT}$, was chosen to compare the influence of B_0 and v_{SEN}.

For the inner measurement position $y15$ in the bulk region of the mold ($z < -45\,\mathrm{mm}$), the immediate observation is that both, an increase in v_{SEN} and in B_0, lead to an increase in the azimuthal velocity. This also applies to the area below the surface, where a change in the flow speed has a significantly stronger effect with regard to flow intensification. The behavior at the outer measurement location $y30$ (Fig. 10 a)) is similar, however, the velocities with applied RMF at $z \leq -200\,\mathrm{mm}$ and different flow speeds (cf. orange and red curve) differ only insignificantly. It is even observable, that the velocities at lower v_{SEN} (orange line) are slightly higher and the zone influenced by the RMF reaches further to the top. With respect to the velocities in vicinity of the meniscus it can be noted that the velocity increase arising from the application of the RMF is higher for the lower v_{SEN} (blue to orange) than for the higher flow speed in the SEN (green to red curve).

3.2.3 Horizontal mold flow under the influence of a counter-rotating RMF

The measurements presented in this section focus on the effect of the stirring direction of the EMS. In Fig. 11 the time-averaged velocities $u_{x0,y15}$ and $u_{x0,y30}$ at $v_{\mathrm{SEN}} \approx 2.1\,\mathrm{m/s}$ with and without the application of electromagnetic stirring in both directions are shown. A positive value of the magnetic flux density B_0 indicates the application of an RMF rotating in the same direction as the swirling flow driven by the GYRONOZZLE, while negative values indicate an applied RMF in opposite direction.

The velocities $u_{x0,y15}$ near the meniscus are almost the same for $B_0 \geq 0$ with values around $-220\,\mathrm{mm/s}$ at $z \geq -25\,\mathrm{mm}$. In contrast, a counter-rotating RMF ($B_0 < 0$) has a braking effect resulting in a remarkable decrease of the velocities near the free surface. This effect is less pronounced at $y30$, which results in $|u_{x0,y15}| \leq |u_{x0,y30}|$ under the meniscus for counter rotating RMFs ($B_0 < 0$) in contrast to $|u_{x0,y15}| \geq |u_{x0,y30}|$ for $B_0 \geq 0$ (cf. Figs. 8 and 9).

For vertical positions below the SEN the counter-rotating RMF effectively brakes the swirling flow induced by the GYRONOZZLE or even induces velocities in the opposite direction. Reversal points of the flow direction were found at $z \approx -300\,\mathrm{mm}$ for a moderate RMF at $B_0 = -7.5\,\mathrm{mT}$ and at $z \approx -120\,\mathrm{mm}$ for the higher $B_0 = -18.3\,\mathrm{mT}$.

A secondary aspect is that the stronger counter-rotating RMF ($B_0 = -18.3\,\mathrm{mT}$) results in smaller absolute velocities in the center of the mold at $y15$ compared to the case where the RMF is applied in the same direction ($u_{x0,y15} \approx 60\,\mathrm{mm/s}$ compared to approx. $-120\,\mathrm{mm/s}$), whereas the absolute values of the velocity at the peripheral position $y30$ are much more similar ($u_{x0,y30} \approx 130\,\mathrm{mm/s}$ compared to approx. $-160\,\mathrm{mm/s}$).

3.3 Measurements of the vertical velocities

The vertical velocity component w has been measured on two cylindrical lateral surfaces at $r15$ and $r30$ in the vicinity of port P3 (see Fig. 3). Fig. 12 shows contour plots of the time-averaged vertical velocity distribution w until a depth of $z = -200\,\mathrm{mm}$ without RMF (a, b) and with a counter-stirring RMF of $B_0 = -18.3\,\mathrm{mT}$ (c, d). At first glance, it becomes obvious that the 90°-symmetry of the GYRONOZZLE results in a related symmetry of the vertical flow structures.

In Fig. 12 a) and c), showing the inner lateral surface at $r15$, three different areas of alternating up and down flows can be distinguished. This general subdivision is not significantly changed by the magnetic field application. While a narrow band below the free surface ($z > -25\,\mathrm{mm}$) is covered by a descending flow, a pronounced upward flow occurs in the region below the SEN and next to the ports down to a depth of approx. $z = -120\,\mathrm{mm}$. Below this position, until the end of the measuring range, again only negative velocities are observed.

A completely different flow structure appears at $r30$ (Figs. 12 b) and d)). The clear threefold division of the flow field over the height as observed at $r15$ is no longer recognizable

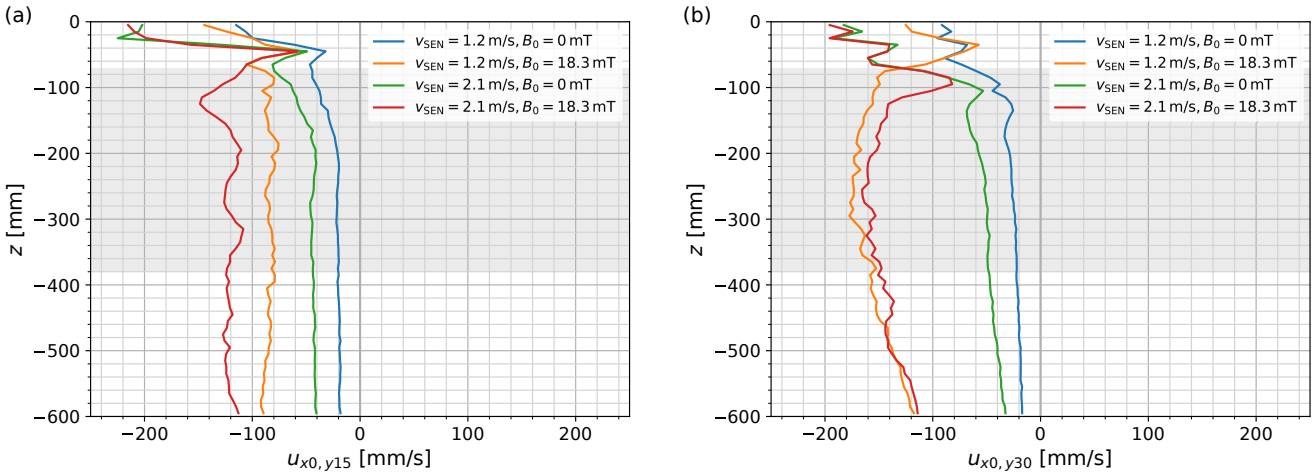

Fig. 10 $u_{x0,y15}$ and $u_{x0,y30}$ with $v_{SEN} \approx 1.2\,\mathrm{m/s}$ and $2.1\,\mathrm{m/s}$, with and without $B_0 = 18.3\,\mathrm{mT}$ measured at a) $y = 15\,\mathrm{mm}$ and b) $y = 30\,\mathrm{mm}$.

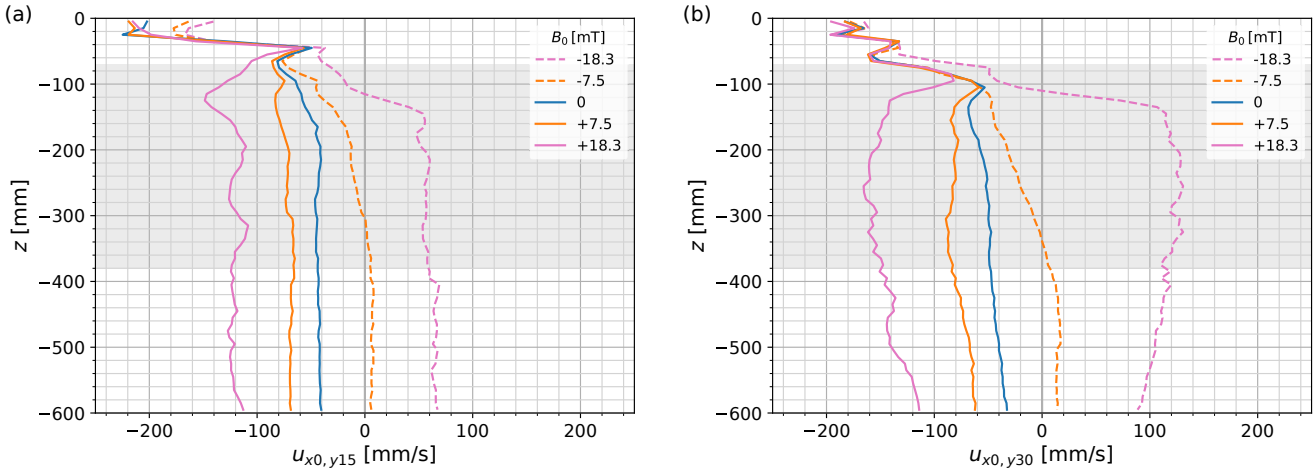

Fig. 11 Time-averaged velocities $u_{x0,y15}$ and $u_{x0,y30}$ with $v_{SEN} \approx 2.1\,\mathrm{m/s}$ and stirring in both directions with different magnetic flux densities B_0 at a) $y = 15\,\mathrm{mm}$ and b) $y = 30\,\mathrm{mm}$.

here. The region below the SEN is clearly dominated by a downward flow, while in the zone of the jets and in the overlaying area up to the free surface, up and down movements alternate periodically. The upward flow seems to reach the free surface, although due to the necessary immersion depth of the UDV sensors and their near-field characteristics, no data for the velocity is available directly under the free surface.

It is noteworthy that the counter-rotating RMF barely changes the general pattern of the vertical flow. Any potential modifications on the inner radius $r15$ are really negligible (see Fig. 12 a) and c)). Obviously, at this position, the inertial forces associated with the exiting jets are so large that electromagnetic stirring can not cause any significant effects here. This behavior changes with increasing radial and axial distance from the nozzle. The RMF rotates in mathematically negative direction which corresponds to a direction of the electromagnetic force from right to left in the plots. This has consequences especially for the structures below the SEN which are deflected in the direction of the electromagnetically driven flow. In particular, a second part of the jet appears to be separated from the actual jet as a single structure shifted in the direction of the RMF to approx. $\varphi = 162°$, $z = -80\,\mathrm{mm}$ (see Fig. 12 d)). Compared to the flow driven solely by the GYRONOZZLE (Fig. 12 b)), the upward flow in the case of the counter-stirring RMF is enlarged and extends from positions under the jets to the free surface. The highest downward velocities in the lower part of the mold are moved from the outside position ($r30$) towards the inside ($r15$) compared to the case without RMF.

Fig. 13 shows magnified sections from Fig. 12 a) and b) to obtain a better impression of the jets. Both plots are scaled equally and contain the projected representation of the

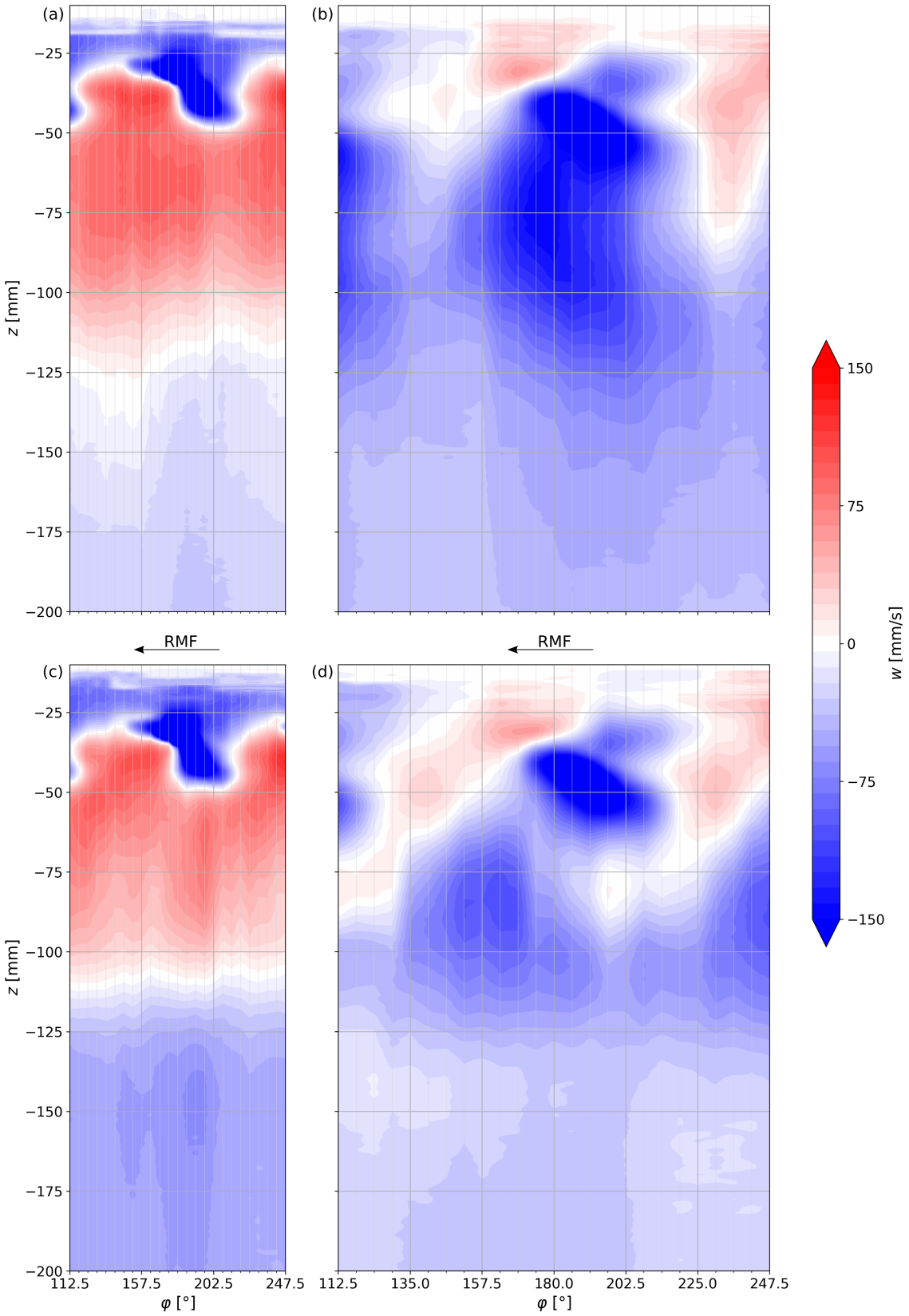

Fig. 12 Time-averaged lateral surface contour plots of the vertical velocity component w in the mold at a SEN velocity of $v_{\mathrm{SEN}} \approx 2.1\,\mathrm{m/s}$ without RMF (a, b) and with the application of a counter-stirring RMF of $B_0 = -18.3\,\mathrm{mT}$ (c, d). View from the outside of the mold at a,c) $r15$ and b,d) $r30$.

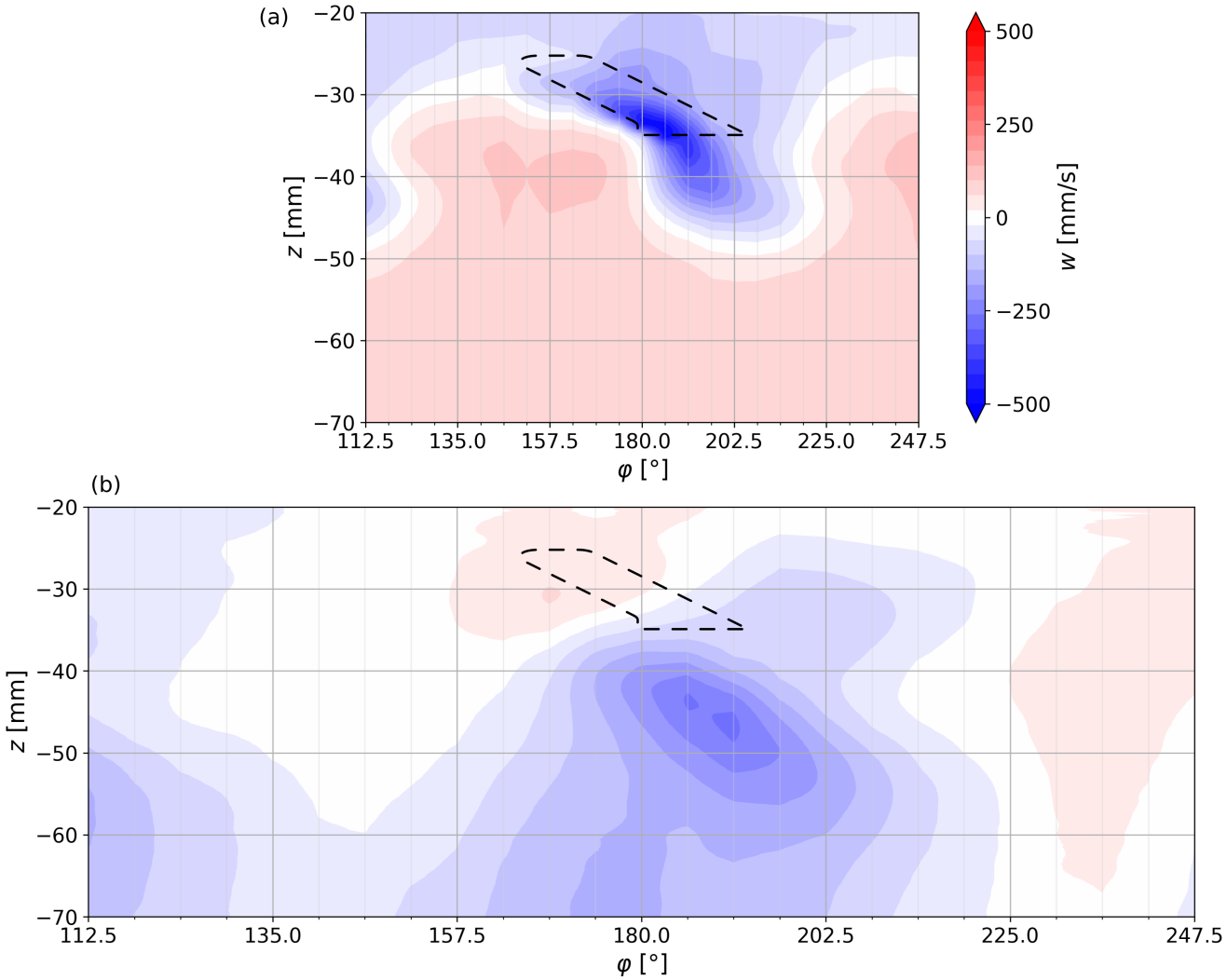

Fig. 13 Time-averaged lateral surface contour plots of the vertical velocity component w in the vicinity of the free surface at port P3 with a SEN velocity of $v_{\mathrm{SEN}} \approx 2.1\,\mathrm{m/s}$ without RMF. View from the outside of the mold at a) $r = 15\,\mathrm{mm}$ and b) $r = 30\,\mathrm{mm}$.

geometry of the port outlet on the respective lateral surface at $r = 10\,\mathrm{mm}$.

The contour plot for the inner lateral surface at $r15$ (Fig. 13 a)) shows the appearance of high negative (downward) velocities in an area corresponding to the position of the jet exiting from port P3. It can be seen that the image of the jet is largely consistent with the shape of the port geometry. It is interesting to note that a significant part of the jet leaves the nozzle almost vertically, probably due to the special design of the outlet with the distinctive vertical edge. In direct vicinity of the jet, opposing positive (upward) velocities are visible, which is equivalent to the occurrence of a high velocity gradient and a shear flow especially at $\varphi = 180° \pm 10°$ between $z = -30\,\mathrm{mm}$ and $-45\,\mathrm{mm}$. At $r30$ (Fig. 13 b)) the jet has traveled a longer distance from its port into the measurement plane and appears as an ellipsoid with its center at $\varphi \approx 190°$ and $z = -45\,\mathrm{mm}$.

4 Discussion

4.1 Assumptions regarding the 3-dimensional structure of the flow

On the basis of all previously presented results obtained by flow measurements of the horizontal and vertical velocity components, it can be tried to qualitatively reconstruct a rough image of the three-dimensional flow structure generated by the GYRONOZZLE.

At first, we look at the vertical velocities recorded for both the $r15$ and $r30$-positions at $\varphi = 180°$ corresponding to the position of port P3. Fig. 14 contains the corresponding time-averaged vertical velocity profiles and a schematic drawing illustrating the derived flow pattern in a rz-plane at $\varphi = 180°$. The jet captured by the two UDV measurement lines exhibits maximum vertical velocities of

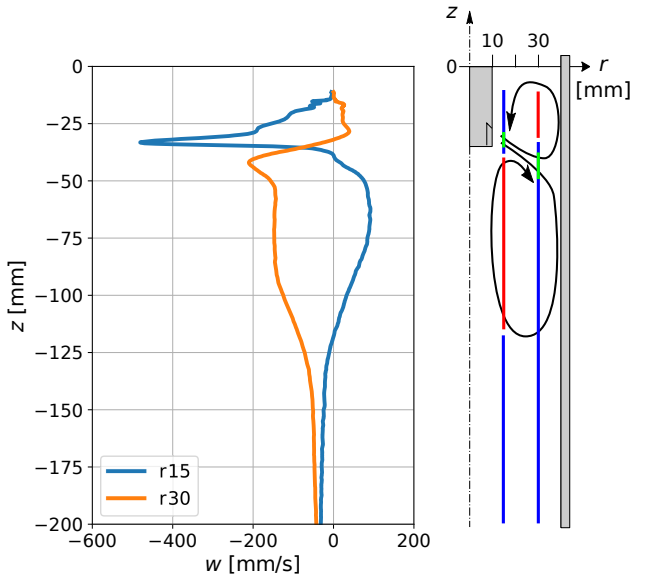

Fig. 14 Time averaged velocity profiles of the vertical velocity component w along the mold height z at $\varphi = 180°$, $r = 15\,\text{mm}$ and $r = 30\,\text{mm}$ at $v_{\text{SEN}} \approx 2.1\,\text{m/s}$ without RMF, as well as a schematic representation of the two roll flow structure that can be conducted from this measurement.

$w_{r15} = -480\,\text{mm/s}$ at $z = -32\,\text{mm}$ and $w_{r30} = -210\,\text{mm/s}$ at $z = -42\,\text{mm}$, respectively. Assuming a correlation of the positions of the maximum velocities and the core of the jet, one can deduce that the jet flows downwards into the mold at an angle of approx. 56° with respect to the z-axis.

After impinging the side wall each jet is split into two parts: One part flows upwards to the free surface along the mold wall and then inwards under the free surface. In this way an upper circulation roll is formed, completed by the downward flow at $r15$. The other part of the jet moves downwards, up to a depth of approx. $z = -120\,\text{mm}$ and creates the lower circulation roll. Such a double-roll flow pattern is well-known from the slab casting process [25]. However, the flow structure considered here is much more complex and fully 3D because the downward movement of the four jets follows a helical path.

Fig. 15 combines vertical and horizontal velocity measurements. The results of measurements carried out at $v_{\text{SEN}} \approx 2.1\,\text{m/s}$ without RMF are shown in three different xy-planes. Additionally to the horizontal velocity measurements at $y15$ and $y30$, the drawings include the vertical velocity measurements at $r15$ and $r30$. Triangles represent the horizontal flow direction. The vertical velocity component is represented by a dot- or a cross symbol, indicating an upward and downward flow, respectively. The size of each symbol indicates the velocity magnitude. Three velocity vectors indicate the flow direction and magnitude in the xy-plane.

The assumption of a quadruple symmetry of the flow in the xy-plane due to the given symmetry of the nozzle allows a quadruple projection of the horizontal measurement lines. That means that additional virtual measuring lines can be obtained at $x15$ and $x30$ without additional measurements by rotating the measured velocity profiles from $y15$ and $y30$ by $-90°$. This leads to the emergence of three virtual intersection points of the measurement lines where the u- and v-component of the velocity can be evaluated according to the following equation:

$$\begin{pmatrix} u(x,y) \\ v(x,y) \end{pmatrix} = \begin{pmatrix} u(x,y) \\ -u(-y,x) \end{pmatrix} \tag{2}$$

Fig. 15a) shows a cross-section close to the free surface of the mold ($z = -15\,\text{mm}$). The horizontal velocity measurements disclose the dominance of the main rotational flow. A slow upward flow at the outside and a downward flow in the center of the mold can be seen in vertical direction. Due to the disturbance introduced to the system by the vertical UDV-probes, which were in direct contact with the liquid metal, the vertical velocities in close vicinity to the transducers can be expected to be higher in the undisturbed system. In Fig. 15b) a cross section just below the ports of the GYRONOZZLE ($z = -45\,\text{mm}$) is depicted, where the two outward pointing vectors at $y15$ show the influence of the jet emerging from port P1. The jet is also visible as downward velocity from the vertical velocity measurements. Between the jets, an upward flow can be seen. This flow transports fluid from $r15$ to $r30$, as indicated by the velocity vector at $x15, y15$. Further down in the mold ($z = -95\,\text{mm}$, Fig. 15c)) the main rotational flow is again visible by the vectors, but with lower magnitude than under the free surface. The vector at $x15, y30$, which is oriented slightly inwards indicates a flow from the outside to the inside as part of the lower roll depicted in Fig. 14.

4.2 Comparison of GYRONOZZLE and single-port nozzle

In Fig. 16 selected results obtained in this study are compared to the findings from a previous work, where the same round mold setup was employed to investigate the case of a standard single-port nozzle under the impact of an RMF [31]. It should be noted, that the flow velocities in the SEN are not identical. The experiment with the single-port-configuration was carried out at $1.4\,\text{m/s}$, whereas $v_{\text{SEN}} \approx 2.1\,\text{m/s}$ in case of the GYRONOZZLE measurements.

It is known that the use of a plain single-port nozzle does not produce any significant swirling flow. The application of an RMF with a field strength of $B_0 = 10.6\,\text{mT}$ is required to produce a comparable rotation rate (e.g. $|u_{x0,y15}| \approx 40\ldots60\,\text{mm/s}$) in the lower part of the mold as achieved by the GYRONOZZLE without RMF. Remarkable differences between the two cases become apparent in the upper part of the mold ($z > -300\,\text{mm}$) at $y15$ (Fig. 16 a)). The combination of the single-port nozzle and the RMF leads to significantly lower tangential velocities in the region of the stirrer, while much higher velocities were measured at the free surface.

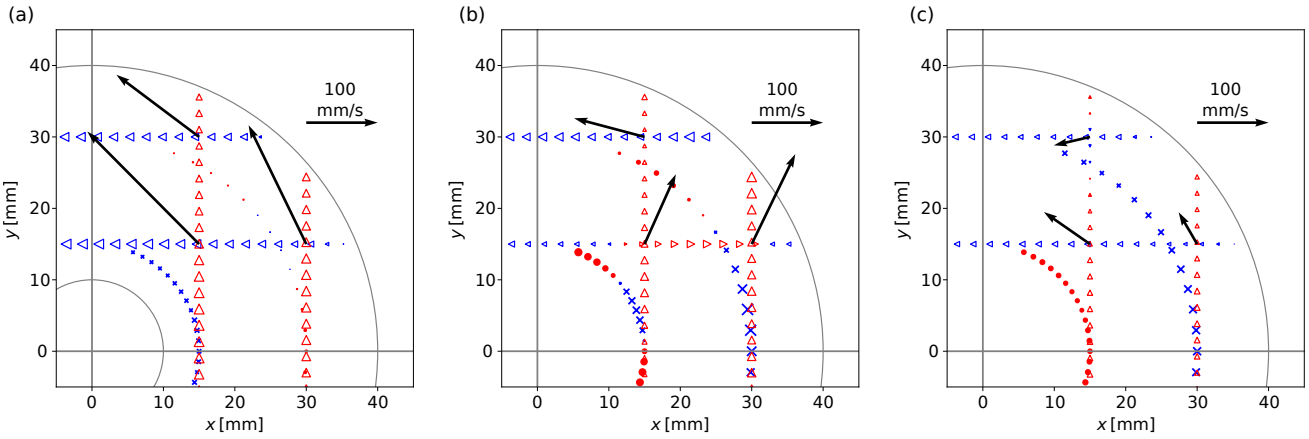

Fig. 15 Combined representation of time-averaged horizontal and vertical measurements in xy-planes with $v_{\mathrm{SEN}} \approx 2.1\,\mathrm{m/s}$ without RMF at a) $z = -15\,\mathrm{mm}$, b) $-45\,\mathrm{mm}$ and c) $-95\,\mathrm{mm}$. Triangles depict the horizontal flow direction, while vertical velocity components are shown as x (downward) or dot (upward). The size of each symbol represents the respective velocity magnitude at that point. A vector representation of the velocities in the xy-plane is shown at the crossing of two horizontal velocity measurement lines.

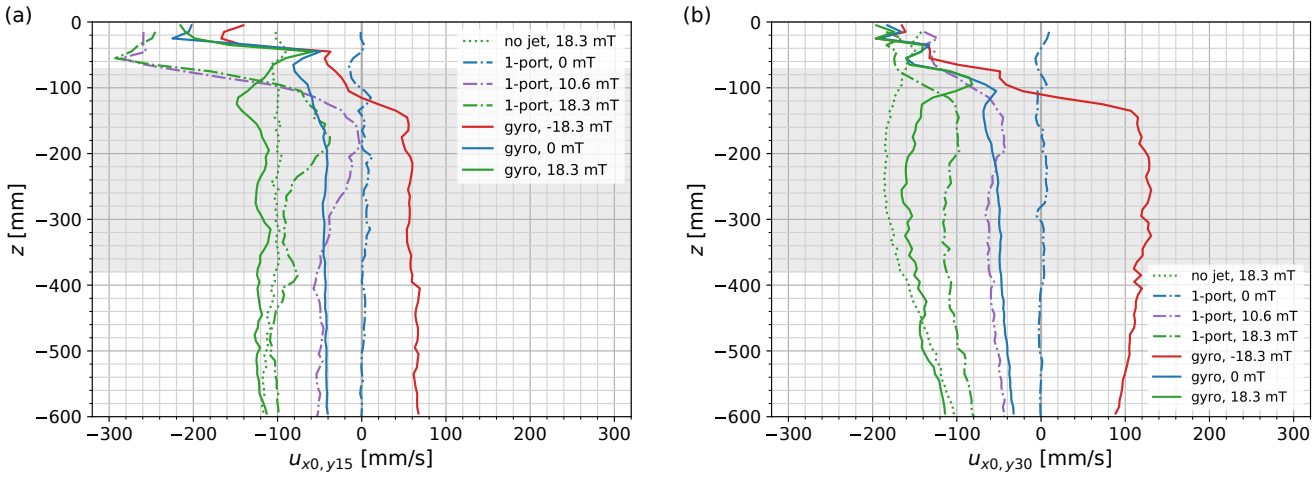

Fig. 16 Comparison of the time-averaged horizontal velocities $u_{x0,y15}$ and $u_{x0,y30}$ obtained by a GYRONOZZLE with selected results of a single-port nozzle from [31] at a) $y = 15\,\mathrm{mm}$ and b) $y = 30\,\mathrm{mm}$.

Such pronounced axial gradients of the swirling flow arise from the axial transport of angular momentum by the secondary meridional flow [31]. In contrast, the vertical profile of the azimuthal flow of the GYRONOZZLE remains almost uniform in the range between $z = -600\,\mathrm{mm}$ and $-100\,\mathrm{mm}$. In addition, the tangential flow at the free surface is considerably smaller compared to the single-port nozzle with RMF. This finding leads to the conclusion that the complex flow around the GYRONOZZLE ports significantly disturbs the meridional flow and restricts the transport of angular momentum. In other words, the GYRONOZZLE with the four jets causes a kind of "shielding"-effect, suppressing the momentum transport from the electromagnetic stirrer to the free surface region. At the outer radial position at $y30$ (Fig. 16 b)), however, the differences between the GYRONOZZLE and the single-port nozzle with superimposed RMF at 10.6 mT are much smaller.

Furthermore, the operation of both nozzle types with a superimposed RMF ($B_0 = 18.3\,\mathrm{mT}$) applied in the same direction as the swirl induced by the GYRONOZZLE is compared. The velocities near the free surface obtained by the GYRONOZZLE at $y15$ are lower than in the case of the single-port nozzle. On the other hand, the GYRONOZZLE achieves higher rotation rates in the strand below the SEN. At $y30$ the velocities under the surface are in both cases similar, but the velocities in the bulk are higher for the GYRONOZZLE.

In comparison with the velocities obtained in a stirred cylindrical column, where the flow through the SEN is zero and therefore no jet is present, it can be observed, that the velocities achieved by the GYRONOZZLE with electromag-

netic stirrer are larger (at $y15$) or close to (at $y30$) those achieved by the stirrer alone, while the velocities of the single-port nozzle are always lower. This behavior demonstrates the supporting effect of the GYRONOZZLE with respect to the swirling flow in the mold.

The configuration of the GYRONOZZLE with a counter-rotating RMF produces a unique flow structure. The fluid regions at the free surface and in the lower part of the mold rotate in opposing directions. Compared to the combination of a single-port nozzle with electromagnetic stirring this variant reduces the swirling velocities at the free surface, especially at $y15$.

4.3 Potential impact on the casting process

In the following section we discuss the potential impact and consequences on the casting process.

The demands on the flow in the SEN and the mold are manifold, although in detail it is often not clear how an optimal flow structure should look like. An important requirement is the limitation of the immersion depth of the jet into the mold. The GYRONOZZLE releases four jets, which move obliquely downward towards the side wall of the mold. The value of the exit angle is between 50° and 60°. The vertical extent of the flow region dominated by the jet, which in turn is an indication for the penetration depth of the jet, scales with the flow rate, i.e. with v_{SEN}. For the maximum value of $v_{\mathrm{SEN}} \approx 2.1\,\mathrm{m/s}$ we found a measurable impact of the jets to a depth of about $z = -125\,\mathrm{mm}$ corresponding to a distance of 90 mm below the lower edge of the GYRONOZZLE. This is a clear advantage with respect to a single-port nozzle at a comparable flow rate.

The flow conditions in the region just beneath the free surface is of great importance in terms of product quality. A veritable flow is necessary to guarantee a sufficient heat and mass transfer near the meniscus. However, a too strong and violent flow has to be avoided because it increases the risk of entrainment of gas or inclusions from the free surface. It was shown by our previous study [31] that the combination of a single-port nozzle and rotary stirring in the mold produces very high velocities near the surface and might create intense vortexes near the nozzle which in the real industrial process are prone to entrain slag into the strand. The fact that the rotational velocities above the stirrer even more than clearly exceed those in the area of the stirrer can be explained by the angular momentum transport by the secondary flow. This transport of angular momentum occurs for any configuration with an axial gradient of the swirling rate and is significantly enhanced by the superimposed jet aligned in vertical direction. In case of the GYRONOZZLE such a transport of angular momentum also occurs between the nozzle region and the near surface region which is demonstrated by the high azimuthal velocities close to the surface (see Figs. 7 or 8). However, the use of a GYRONOZZLE could be beneficial with respect to slag entrainment, since the observed velocities under the free surface are considerably lower compared to a single-port SEN with RMF, as seen in Fig. 16. This even applies to the combination of GYRONOZZLE and RMF. Thus, this study gave the new and interesting finding that the flow generated by the GYRONOZZLE effectively inhibits the angular momentum transport between the electromagnetic stirrer and the surface region. This phenomenon can be understood as a "shielding"-effect, caused by the inertia of the four jets. Accordingly, this effect becomes stronger with increasing velocity in the SEN corresponding to a higher kinetic energy of the jets (Fig. 10).

The flow field in the jet region appears to be rather complicated. Such a structure of strong velocity gradients and frequent changes of direction should provide a good mixing. In particular, measurements of the vertical velocity component reveals alternating domains of descending and ascending flows in the nozzle region, the latter reaching to the surface. This flow is supposed to support the transport of inclusions to the surface where they could be separated from the melt and remain in the slag layer.

The general question of whether an electromagnetic stirrer can be completely replaced by a GYRONOZZLE is difficult to answer. The present study demonstrates that the GYRONOZZLE is able to generate the main feature of a M-EMS, namely, a stable and persistent rotating flow in the mold. And as just stated, in comparison to the combination of single-port nozzle and M-EMS the GYRONOZZLE configuration also seems to be less dangerous in terms of a possible exaggeration of the swirling flow in the near surface region. However, a limitation could be seen in the fact that the swirling flow in the mold and the ratio of the rotation rates in the mold and at the surface are not freely controllable during the process, but instead, apart from the geometry, depend only on the set velocity in the nozzle, v_{SEN}. Here, the combined use of GYRONOZZLE and M-EMS results in much more flexibility. For instance, the application of a co-rotating RMF opens the possibility to achieve high velocities in the bulk, while the increase of the velocities under the free surface remains moderate. The relation of velocities in the bulk to those at the free surface is almost freely selectable by varying the parameters casting speed and electromagnetic flux density of the stirrer.

The combination of the GYRONOZZLE with a counter-rotating RMF does not seem obvious from the outset, but might lead to an intensified mixing especially in the region of the mold where the flow direction changes. The removal of particles from the strand might be further improved by counter-stirring compared to the application of a co-rotating RMF, as the upward flow at the outside of the mold extends deeper into the mold (see Fig. 12). A very attractive and important feature is the capability for a flexible and indepen-

dent control of the swirling flows both in the mold and in the meniscus region. Despite intense stirring in the deeper mold a distinct reduction of the velocities beneath the free surface can be achieved which is beneficial to prevent inclusion entrainment by surface vortexes (cf. [31]). For that purpose, Chang et al. [1] proposed a special arrangement of two rotating magnetic fields installed one on top of the other at the mold. The direction of rotation of the stirrer in the meniscus region is opposite to that of the main stirrer below. GYRONOZZLE and counter-rotating RMF enable the same possibilities for effective flow control in the mold with considerably less technical effort.

5 Conclusions

An experimental study is presented considering the effect of a swirling flow submerged entry nozzle (SEN), the RHI Magnesita GYRONOZZLE, for the fluid flow in continuous casting of blooms and billets. A liquid metal model has been used in order to investigate the operation conditions for the GYRONOZZLE also in the case when electromagnetic stirring is applied simultaneously. The experiments were conducted in a circular mold equipped with an electromagnetic stirrer (M-EMS) as part of the Mini-LIMMCAST facility at HZDR [26]. Horizontal and vertical velocity components were measured by means of the Ultrasound Doppler Velocimetry (UDV) to detect the flow structures inside the mold.

The experimental results have lead to the following conclusions:

1. The application of the GYRONOZZLE produces an intense rotational flow in the mold, with the highest velocities occurring in the vicinity of the free surface and the mean velocities rising linearly with an increasing liquid flow rate through the SEN.
2. Three areas with different flow structures exist, namely a fast rotating zone near the free surface, a complex three-dimensional flow around the nozzle ports which is dominated by the inertia of the emerging jets, and a moderately rotating core in the bottom part of the mold.
3. A helical double-role flow pattern has been identified, where downward flowing fluid from the outside of the mold moves to the center and upwards. Between the jets the flow moves from the center to the outside of the free surface. In the casting process this flow pattern might wash non-metallic inclusions off the solidified strand shell and transport them to the free surface where they could be extracted from the melt by the slag layer.
4. The jets emerging from the GYRONOZZLE cause a complex and highly turbulent flow which effectively prevents the angular momentum transfer from the M-EMS zone below the nozzle towards the free surface. This "shielding"-effect is stronger for higher velocities in the SEN and therefore moves the region affected by the stirrer further downwards. It is very beneficial to limit the maximum rotation velocities at the free surface which otherwise bear the risk of slag or gas entrainment.
5. The combined use of the GYRONOZZLE with co-rotating electromagnetic stirring around the mold creates an intense rotational flow in the lower part of the mold. While the magnitude of this flow near the side wall of the mold increases with increasing magnetic flux density of the stirrer, a saturation effect is observed in the center of the mold. Increased stirring causes only minor changes to the rotational flow at the free surface. The rotational velocities in the mold obtained by the GYRONOZZLE and RMF are above those of a single-port SEN with the same RMF strength.
6. A GYRONOZZLE operated with a counter-rotating RMF creates a unique flow pattern with opposing rotational flow directions in the upper and lower part of the mold. With this operational mode the velocities under the free surface are reduced.

When a GYRONOZZLE or other multi-port SEN designs are used in a non axis-symmetric mold, the positioning of the nozzle ports towards the walls of the mold is an important parameter for the developing flow in mold and strand and therefore for the product quality. It would therefore be worth continuing experiments focusing on flow measurements in a liquid metal model with varying geometries (e.g. square cross sections) in further studies.

Acknowledgements The HZDR authors are grateful to RHI Magnesita for supplying a 3D printed model of the GYRONOZZLE and for a financial contribution to the research project.

References

1. Chang, F.C., Hull, J.R., Beitelman, L.: Simulation of flow control in the meniscus of a continuous casting mold with opposing alternating current magnetic fields. Metall. Mater. Trans. B **35**(6), 1129–1137 (2004). DOI 10.1007/s11663-004-0069-6
2. Eckert, S., Cramer, A., Gerbeth, G.: Velocity Measurement Techniques for Liquid Metal Flows. In: R. Moreau (ed.) Magnetohydrodynamics, vol. 80, pp. 275–294. Springer Netherlands, Dordrecht (2007). DOI 10.1007/978-1-4020-4833-3_17
3. Evonik Industries AG: Technical Information PLEXIGLAS® (2013)
4. Franke, S., Büttner, L., Czarske, J., Räbiger, D., Eckert, S.: Ultrasound Doppler system for two-dimensional flow mapping in liquid metals. Flow Meas. Instrum. **21**(3), 402–409 (2010). DOI 10.1016/j.flowmeasinst.2010.05.001

5. Franke, S., Lieske, H., Fischer, A., Büttner, L., Czarske, J., Räbiger, D., Eckert, S.: Two-dimensional ultrasound Doppler velocimeter for flow mapping of unsteady liquid metal flows. Ultrasonics **53**(3), 691–700 (2013). DOI 10.1016/j.ultras.2012.10.009
6. Hackl, G., Nitzl, G., Tang, Y., Eglsäer, C., Chalmers, D.: Innovative Flow Control Refractory Products for the Continuous Casting Process. In: AISTech 2015 Proceedings, pp. 2436–2442. Association for Iron & Steel Technology (2015)
7. Hackl, G., Tang, Y., Nitzl, G., Schurmann, D., Willers, B., Eckert, S.: Gyro Nozzle – An Innovative Submerged Entry Nozzle Design for Billet and Bloom Casting. In: AISTech 2018 Proceedings, pp. 1655–1662. Association for Iron & Steel Technology, Philadelphia (2018)
8. Ho, C.Y., Chu, T.K.: Electrical resistivity and thermal conductivity of nine selected AISI stainless steels. Tech. Rep. 45, Cindas, Purdue University, West Lafayette (1977)
9. Javurek, M., Barna, M., Gittler, P., Rockenschaub, K., Lechner, M.: Flow Modelling in Continuous Casting of Round Bloom Strands with Electromagnetic Stirring. Steel Res. Int. **79**(8), 617–626 (2008). DOI 10.1002/srin.200806174
10. Jimbo, I., Cramb, A.W.: The density of liquid iron-carbon alloys. Metall. Trans. B **24**(1), 5–10 (1993). DOI 10.1007/BF02657866
11. Korolczuk-Hejnak, M., Migas, P., Ślęzak, W.: Determination of the liquid steel viscosity curves using a high temperature rheometer. J. Phys.: Conf. Ser. **602**, 012,037 (2015). DOI 10.1088/1742-6596/602/1/012037
12. Krautkrämer, J., Krautkrämer, H.: Werkstoffprüfung mit Ultraschall, 5 edn. Springer, Berlin, Heidelberg (1986). DOI 10.1007/978-3-662-10909-0
13. Li, D., Su, Z., Chen, J., Wang, Q., Yang, Y., Nakajima, K., Marukawa, K., He, J.: Effects of Electromagnetic Swirling Flow in Submerged Entry Nozzle on Square Billet Continuous Casting of Steel Process. ISIJ Int. **53**(7), 1187–1194 (2013). DOI 10.2355/isijinternational.53.1187
14. Li, Z., Mukai, K., Zeze, M., Mills, K.C.: Determination of the surface tension of liquid stainless steel. J. Mater. Sci. **40**(9-10), 2191–2195 (2005). DOI 10.1007/s10853-005-1931-x
15. Morley, N.B., Burris, J., Cadwallader, L.C., Nornberg, M.D.: GaInSn usage in the research laboratory. Rev. Sci. Instrum. **79**(5), 056,107 (2008). DOI 10.1063/1.2930813
16. Ni, P., Ersson, M., Jonsson, L.T.I., Zhang, T.a., Jönsson, P.G.: Numerical Study on the Influence of a Swirling Flow Tundish on Multiphase Flow and Heat Transfer in Mold. Metals **8**(5), 368 (2018). DOI 10.3390/met8050368
17. Ni, P., Jonsson, L.T.I., Ersson, M., Jönsson, P.G.: Application of a Swirling Flow Producer in a Conventional Tundish during Continuous Casting of Steel. ISIJ Int. **57**(12), 2175–2184 (2017). DOI 10.2355/isijinternational.ISIJINT-2017-377
18. Ni, P., Jonsson, L.T.I., Ersson, M., Jönsson, P.G.: Non-Metallic Inclusion Behaviors in a New Tundish and SEN Design Using a Swirling Flow during Continuous Casting of Steel. Steel Res. Int. **88**(3), 1600,155 (2017). DOI 10.1002/srin.201600155
19. Ni, P., Wang, D., Jonsson, L.T.I., Ersson, M., Zhang, T.a., Jönsson, P.G.: Numerical and Physical Study on a Cylindrical Tundish Design to Produce a Swirling Flow in the SEN During Continuous Casting of Steel. Metall. Mater. Trans. B **48**(5), 2695–2706 (2017). DOI 10.1007/s11663-017-1057-y
20. Plevachuk, Y., Sklyarchuk, V., Eckert, S., Gerbeth, G., Novakovic, R.: Thermophysical Properties of the Liquid Ga–In–Sn Eutectic Alloy. J. Chem. Eng. Data **59**(3), 757–763 (2014). DOI 10.1021/je400882q
21. Signal Processing S. A.: DOP3000-3010 Series User's Manual. Switzerland (2017)
22. Spitzer, K.H., Dubke, M., Schwerdtfeger, K.: Rotational electromagnetic stirring in continuous casting of round strands. Metall. Trans. B **17**(1), 119–131 (1986). DOI 10.1007/BF02670825
23. Su, Z.J., Chen, J., Nakajima, K., He, J.C.: Criterion for Dendrite Fragmentation of Carbon Steel under Imposition of Linear Travelling EMS. Steel Res. Int. **80**(11), 824–831 (2009). DOI 10.2374/SRI09SP014
24. Sun, H., Zhang, J.: Macrosegregation Improvement by Swirling Flow Nozzle for Bloom Continuous Castings. Metall. Mater. Trans. B **45**(3), 936–946 (2014). DOI 10.1007/s11663-013-9999-1
25. Thomas, B.G.: Fluid flow in the mold. In: Making, Shaping and Treating of Steel, vol. 5, 11 edn., pp. 1–41. AISE Steel Foundation, Pittsburgh (2003)
26. Timmel, K., Eckert, S., Gerbeth, G., Stefani, F., Wondrak, T.: Experimental Modeling of the Continuous Casting Process of Steel Using Low Melting Point Metal Alloys - the LIMMCAST Program. ISIJ Int. **50**(8), 1134–1141 (2010). DOI 10.2355/isijinternational.50.1134
27. Timmel, K., Kratzsch, C., Asad, A., Schurmann, D., Schwarze, R., Eckert, S.: Experimental and Numerical Modeling of Fluid Flow Processes in Continuous Casting: Results from the LIMMCAST-Project. IOP Conf. Ser.: Mater. Sci. Eng. **228**, 012,019 (2017). DOI 10.1088/1757-899X/228/1/012019
28. Timmel, K., Miao, X., Wondrak, T., Stefani, F., Lucas, D., Eckert, S., Gerbeth, G.: Experimental and numerical modelling of the fluid flow in the continuous casting of steel. Eur. Phys. J. Special Topics **220**(1), 151–166 (2013). DOI 10.1140/epjst/e2013-01804-5

29. Tsukaguchi, Y., Hayashi, H., Kurimoto, H., Yokoya, S., Marukawa, K., Tanaka, T.: Development of Swirling-flow Submerged Entry Nozzles for Slab Casting. ISIJ Int. **50**(5), 721–729 (2010). DOI 10.2355/isijinternational.50.721
30. Tzavaras, A.A., Brody, H.D.: Electromagnetic stirring and continuous casting - Achievements, problems, and goals. JOM **36**(3), 31–37 (1984). DOI 10.1007/BF03338405
31. Willers, B., Barna, M., Reiter, J., Eckert, S.: Experimental Investigations of Rotary Electromagnetic Mould Stirring in Continuous Casting Using a Cold Liquid Metal Model. ISIJ Int. **57**(3), 468–477 (2017). DOI 10.2355/isijinternational.ISIJINT-2016-495
32. Willers, B., Eckert, S., Michel, U., Haase, I., Zouhar, G.: The columnar-to-equiaxed transition in Pb–Sn alloys affected by electromagnetically driven convection. Mater. Sci. Eng. A **402**(1-2), 55–65 (2005). DOI 10.1016/j.msea.2005.03.108
33. Wondrak, T., Eckert, S., Galindo, V., Gerbeth, G., Stefani, F., Timmel, K., Peyton, A.J., Yin, W., Riaz, S.: Liquid metal experiments with swirling flow submerged entry nozzle. Ironmaking Steelmaking **39**(1), 1–9 (2012). DOI 10.1179/1743281211Y.0000000045
34. Yang, Y., Jönsson, P.G., Ersson, M., Nakajima, K.: Inclusion Behavior under a Swirl Flow in a Submerged Entry Nozzle and Mold. Steel Res. Int. **86**(4), 341–360 (2015). DOI 10.1002/srin.201300462
35. Yang, Y., Jönsson, P.G., Ersson, M., Su, Z., He, J., Nakajima, K.: The Influence of Swirl Flow on the Flow Field, Temperature Field and Inclusion Behavior when Using a Half Type Electromagnetic Swirl Flow Generator in a Submerged Entry and Mold. Steel Res. Int. **86**(11), 1312–1327 (2015). DOI 10.1002/srin.201400330
36. Yokoya, S., Asako, Y., Hara, S., Szekely, J.: Control of Immersion Nozzle Outlet Flow Pattern through the Use of Swirling Flow in Continuous Casting. ISIJ Int. **34**(11), 883–888 (1994). DOI 10.2355/isijinternational.34.883
37. Yokoya, S., Takagi, S., Iguchi, M., Asako, Y., Westoff, R., Hara, S.: Swirling Effect in Immersion Nozzle on Flow and Heat Transport in Billet Continuous Casting Mold. ISIJ Int. **38**(8), 827–833 (1998). DOI 10.2355/isijinternational.38.827
38. Yokoya, S., Westoff, R., Asako, Y., Hara, S., Szekely, J.: Numerical Study of Immersion Nozzle Outlet Flow Pattern with Swirling Flow in Continuous Casting. ISIJ Int. **34**(11), 889–895 (1994). DOI 10.2355/isijinternational.34.889